Int J Adv Manuf Technol (2018) 94:2239–2254
DOI 10.1007/s00170-017-1014-6

ORIGINAL ARTICLE

Performance of a pressurized internal-cooling slotted grinding wheel system

Ruitao Peng[1] · **Xiaofang Huang**[1] · **Xinzi Tang**[1] · **Rui Chen**[1] · **Yunbo Hu**[2]

Received: 12 June 2017 / Accepted: 17 August 2017 / Published online: 6 September 2017

Abstract Internal-cooling technology is an effective cooling method to reduce the temperature in grinding zone and avoid grinding burn for grinding hard-to-cut materials. In order to overcome the technological difficult problems generated by grinding heat in grinding process, such as pull, burns, and surface bonding, a novel method of pressurized internal-cooling was proposed to strengthen the heat dissipation of grinding arc zone. Initially, a pressurized internal-cooling slotted grinding wheel with regular grain distribution was delicately designed with numeric simulation and further validated with a 3D printing model. Subsequently, various parts of the grinding wheel and its supporting fixture were prepared and assembled. Finally, pressurized internal-cooling method and external-cooling method were utilized in grinding nickel-based superalloy, respectively, under the same grinding parameters. The results indicate that the proposed pressurized internal-cooling method, compared with the traditional external-cooling method or other internal-cooling method which only rely on centrifugal force, offers higher heat transfer efficiency, lower grinding temperature and surface roughness, and better surface integrity.

Keywords Pressurized internal-cooling · Regular grain distribution · Nickel-based superalloy · Grinding temperature · Surface quality

✉ Ruitao Peng
pengruitao@xtu.edu.cn

Xiaofang Huang
huangxiaofangcc@163.com

Xinzi Tang
tangxinzi@xtu.edu.cn

Rui Chen
chenrui85@xtu.edu.cn

Yunbo Hu
hyb_cheery@163.com

[1] Engineering Research Center of Ministry of Education for Complex Track Processing Technology and Equipment, School of Mechanical Engineering, Xiangtan University, Xiangtan 411105, People's Republic of China

[2] AECC Hunan South Astronautics Industry Co. LTD., Zhuzhou 412002, People's Republic of China

1 Introduction

Nickel-based superalloy is commonly applied in the gas and steam turbines components and aircraft engine component construction, owing to its high strength, excellent corrosion resistance, and good fatigue resistance, as demonstrated by Ulutan et al. [1] and Ezugwu [2]. In order to obtain good machining quality and high dimensional accuracy, the grinding process is generally arranged at the last stage of machining. Nevertheless, Choudhury et al. [3] found that the grindability of nickel base superalloy was poor. Malkin et al. [4] found high grinding force and grinding temperature existing in the grinding process, and there existed a strong force-thermocouple effect. The coolant was hard to enter the grinding area to cool the wheel-workpiece interface, which resulted in difficulties in guarantying the integrity of machined surface and limited grinding efficiency. Traditionally, the coolant is injected into grinding contact zone for enhancing the heat transfer effect, but the "air barrier" phenomenon caused by the high-speed rotation of the grinding wheel, proposed by Brinksmeier et al. [5], brings about decrease to cooling effect. Consequently, to improve the heat transfer efficiency of the coolant, and to further reduce the temperature of the grinding

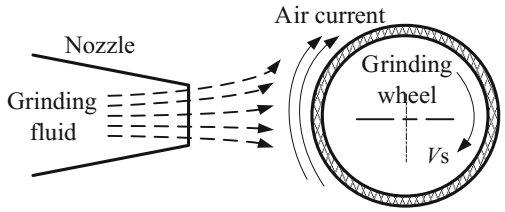

Fig. 1 Schematic diagram of air barrier phenomenon

zone, a new cooling method was proposed, which was of great significance to improve the surface quality of difficult-to-machine materials.

In order to solve problems of traditional cooling technologies, some scholars have done plenty of research on coolant injection technology, such as needle-shaped high-pressure jet cooling, grooved grinding wheel cooling, liquid nitrogen cryogenic cooling, heat pipe cooling, and spray impingement cooling, as studied by Chen et al. [6] and He et al. [7]. Some disadvantages appear, i.e., unstable penetration efficiency, production of eccentric vibration, and the need for special complex nozzle or special coolant, using conventional external spraying cooling. Given this, the internal-cooling method becomes an effective and practical solution. Shi et al. [8] designed an internal-cooling wheel based on centrifugal jet and found that it could reduce the grinding temperature effectively, compared with a plain grinding wheel in grinding nickel-based superalloy. Krzysztof et al. [9] developed an internal-cooling wheel for internal grinding. The experimental results showed that the grinding wheel could improve the utilization of grinding fluid and the heat transfer effect and reduce surface burns to a certain extent. Aurich et al. [10] designed a disk-shaped CBN grinding wheel based on the principle of centrifugal pumps and discovered that both simulation and experimental results demonstrated that the internal-cooling method was beneficial to heat dissipating of the arc zone. Nevertheless, provided that the coolant is transported only through centrifugal force produced by rotation of grinding wheels, not only the utilization rate of coolant will be limited, but the cooling effect will have difficulty to control effectively.

Meanwhile, some advanced methods or technologies have been also applied to reduce greatly grinding temperature, such as creep-feed deep grinding technique, high-efficiency deep grinding technique, brazing technology, and phyllotaxis theory of abrasive distribution. Ding et al. [11] investigated that the grinding zone temperature was merely about 180 °C during creep-feed grinding nickel-based superalloy. Chen et al. [12] found that the developed porous CBN wheels had a promising application in high-efficiency deep grinding nickel-based alloy. Ding et al. [13] indicated that during high-speed shallow grinding of Inconel718 alloy, the grinding forces and temperature with this porous CBN wheel were nearly 20~30% lower than that with the traditional vitrified wheel. The disordered arrangement of the abrasive can reduce the effective utilization rate of the abrasive grains, which directly affects the grinding efficiency of the grinding wheel, as elucidated by Yu et al. [14]. Ding et al. [15] found that grain distribution and working surface patterns had a great influence on the grinding performance of monolayer CBN wheels, but needed to be optimized further. Oliveira et al. [16] found that regular grain distribution could be obtained by automatic exposure technique, and the research has been carried on. The experimental results show that the grinding wheel with regular grain distribution has good grinding performance in conventional grinding process.

Based on the previous research ideas, considering the combination of the grinding fluid pressurization technology, grinding wheel internal-cooling technology, and intermittent grinding technology, a pressurized internal-cooling slotted grinding wheel with regular grain distribution for surface grinding was developed. Structural parameters of grinding wheels were designed and verified, respectively, based on numerical simulation method and 3D printing technology. Pressurized internal-cooling method and external-cooling method were, respectively, utilized in grinding experiments for nickel-based superalloy under the same condition. The influence regularity of rotating speeds and coolant pressure on the grinding temperature and the surface quality was studied.

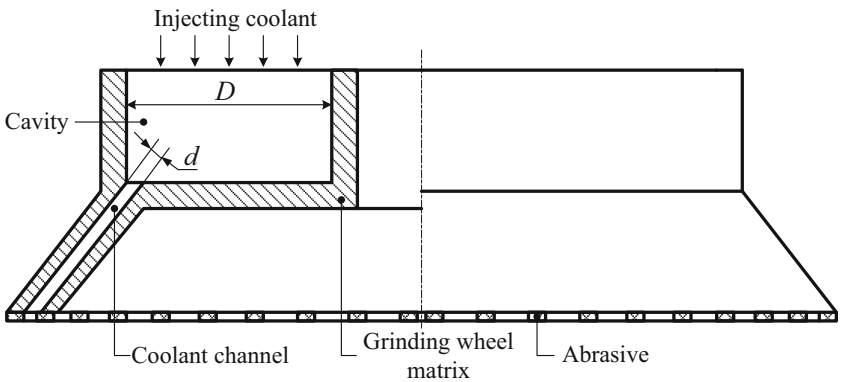

Fig. 2 Schematic diagram of the working principle of the pressure internal-cooling grinding wheel

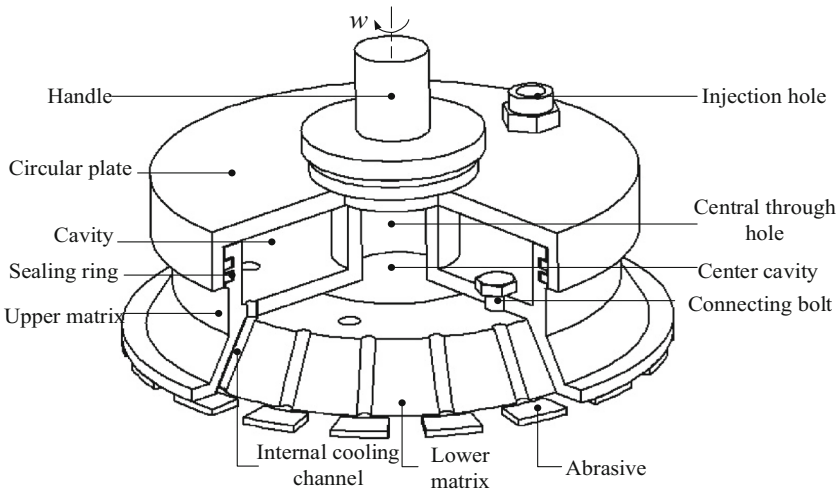

Fig. 3 Schematic diagram of the grinding wheel

2 Work principle of the grinding wheel

As shown in Fig. 1, due to the high-speed rotation of the grinding wheel in grinding, an air boundary layer is formed around the periphery of wheels, which prevents the grinding fluid from entering the grinding arc zone, which is generally called air barrier phenomenon, proposed by Brinksmeier et al. [5]. The higher rotating speed of the grinding wheel is, the greater the air barrier effect appears, the harder for injecting coolant into the grinding zone, which not only seriously affects the processing quality but also limits the grinding efficiency.

A kind of pressurized internal-cooling slotted grinding wheel was designed by Peng et al. [17] and a schematic diagram of the working principle of the grinding wheel as shown in Fig. 2. The pressurized coolant is injected into the grinding wheel cavity, and the difference between the diameter of the injection hole and the diameter of the channel in the cavity leads to the change of pressure in the cavity. Subsequently, under the combined action of external pressure and high-speed centrifugal force, the coolant go through the small coolant channel inside the grinding wheel and is sprayed into grinding arc zone with the higher outlet pressure, thus avoiding the air barrier effect, accelerating heat transfer, and reducing the arc temperature. In the course of the grinding process, the coolant pressure is controlled by a pressure system to effectively control and adjust the outlet pressure and velocity.

3 Design and preparation of the grinding wheel

3.1 Structure design of the pressurized internal-cooling slotted grinding wheel

3.1.1 Design of the grinding wheel substrate

Based on the working principle of the pressurized internal-cooling grinding wheel and the intermittent grinding method,

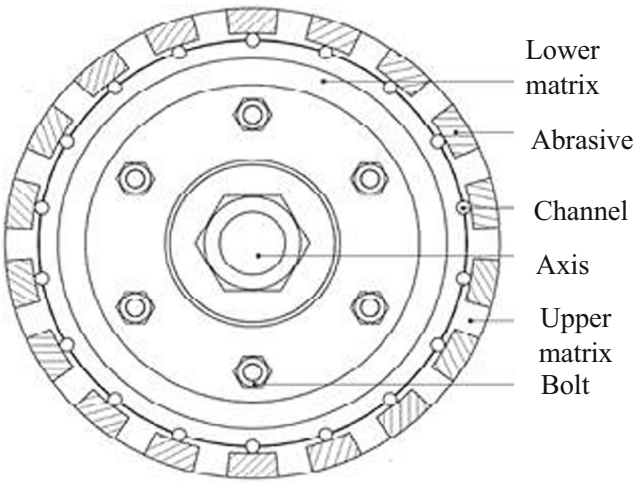

Fig. 4 Schematic diagram of the grinding wheel bottom

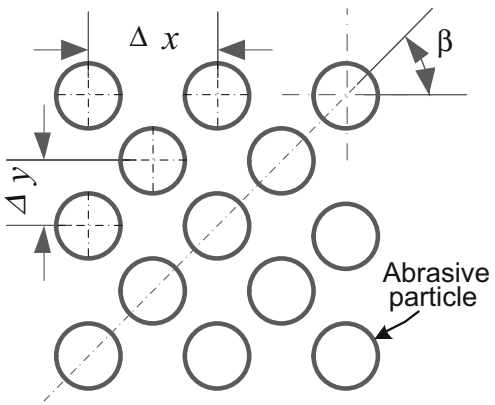

Fig. 5 Schematic diagram of abrasive grains orderly (β is the abrasive arrangement angle, Δx reflects lateral spacing, Δy expresses longitudinal spacing)

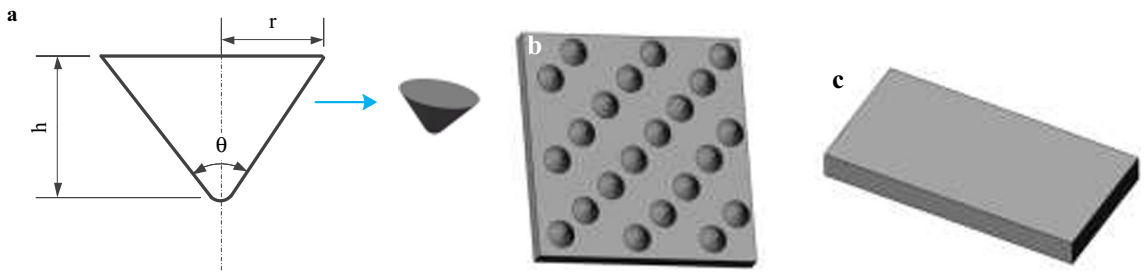

Fig. 6 Model of multiple abrasive and workpiece. **a** CBN abrasive grains. **b** Multi-particle model. **c** Workpiece material"

the structure of the grinding wheel was designed as shown in Fig. 3. The grinding wheel is a bowl-shaped structure, which is composed of upper matrix, lower matrix, and cover. The upper matrix is provided with a central through hole for clamping. The annular cavity and the sealing cover are combined to form a coolant chamber to store the coolant, and a coolant injection hole is arranged on the cover plate. The upper matrix inner wall and the lower matrix outer wall are uniformly distributed with a coolant channel, and matrixes are assembled using bolts to form a closed columnar flow channel. The abrasive particles are uniformly distributed on the lower end face of the upper matrix. Both inlet and outlet of coolant channel are located, respectively, in the coolant chamber of the grinding wheel and the abrasive, and the number of coolant channel is the same as that of the abrasive block.

The 45 steel was utilized as the matrix material of the grinding wheel, and the inner diameter of the grinding wheel was the same as spindle diameter of the machine tool. This paper determined the grinding wheel working face in outer diameter of 150 mm, and internal diameter of 130 mm, considering the influence of grinding parameters on the grinding wheel vibration, energy consumption, and other aspects.

3.1.2 Design of the abrasive arrangement

The slotted grinding wheel changed the grinding cycle characteristics, and the uniform channel was favorable to coolant entering the grinding area. According to the moving heat source model, as illuminated by Malkin et al. [4], the slot number $N\epsilon$ [16, 32] and the groove factor $\eta\epsilon$ [0.5, 0.7] were more reasonable. If the two coefficients are not within the range, a smaller groove factor η will lead to intensifying wheel wear and deteriorating surface roughness of machined workpiece, and a bigger slot number N may more likely result in wheel wear. Furthermore, reasonable slot number N and groove factor η will input more coolant into the grinding area, thereby improving the processing performance. Taking into account the structural strength of the wheel and difficulty degree of machining, the groove factor η and the slot number N were determined, respectively, as 0.6 and 18. So given the influence of height and angle of flow nozzle, the inclined angle of the channel was taken as 60°. The 18 groups of the coolant channel and abrasive block were evenly distributed in the lower end, as shown in Fig. 4.

During the grinding process, each effective abrasive grain distributed on the bottom of the grinding wheel matrix is involved in grinding, and the grinding speed, depth of the abrasive grains, and their arrangement have an important influence on the grinding force, grinding temperature, and workpiece surface quality, as elaborated by Courbon et al. [18]. Regular grains distribution is designed out of abrasive grains angle and spacing under the premise of reasonable selection of the abrasive grain size. The schematic diagram of abrasive grains orderly is shown in Fig. 5. In this paper, according to the research results of Ghosh A et al. [19], the abrasive particle size of #80 and the particle size range of 160~200 μm were selected.

In order to obtain a more reasonable arrangement parameter of abrasive grains, the grinding process of multiple

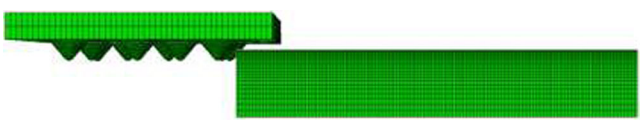

Fig. 7 Finite element model of multi-abrasive grinding

Table 1 Simulation parameters

Sequence number	Arrangement angle β	Lateral spacing Δx/mm	Longitudinal spacing Δy/mm
1	30°	1.0	0.2
2	45°		
3	60°		
4	75°		
5	90°		
6	45°	2.0	0.1
7		1.0	0.2
8		0.66	0.3
9		0.5	0.4
10		0.4	0.5
11		0.33	0.6

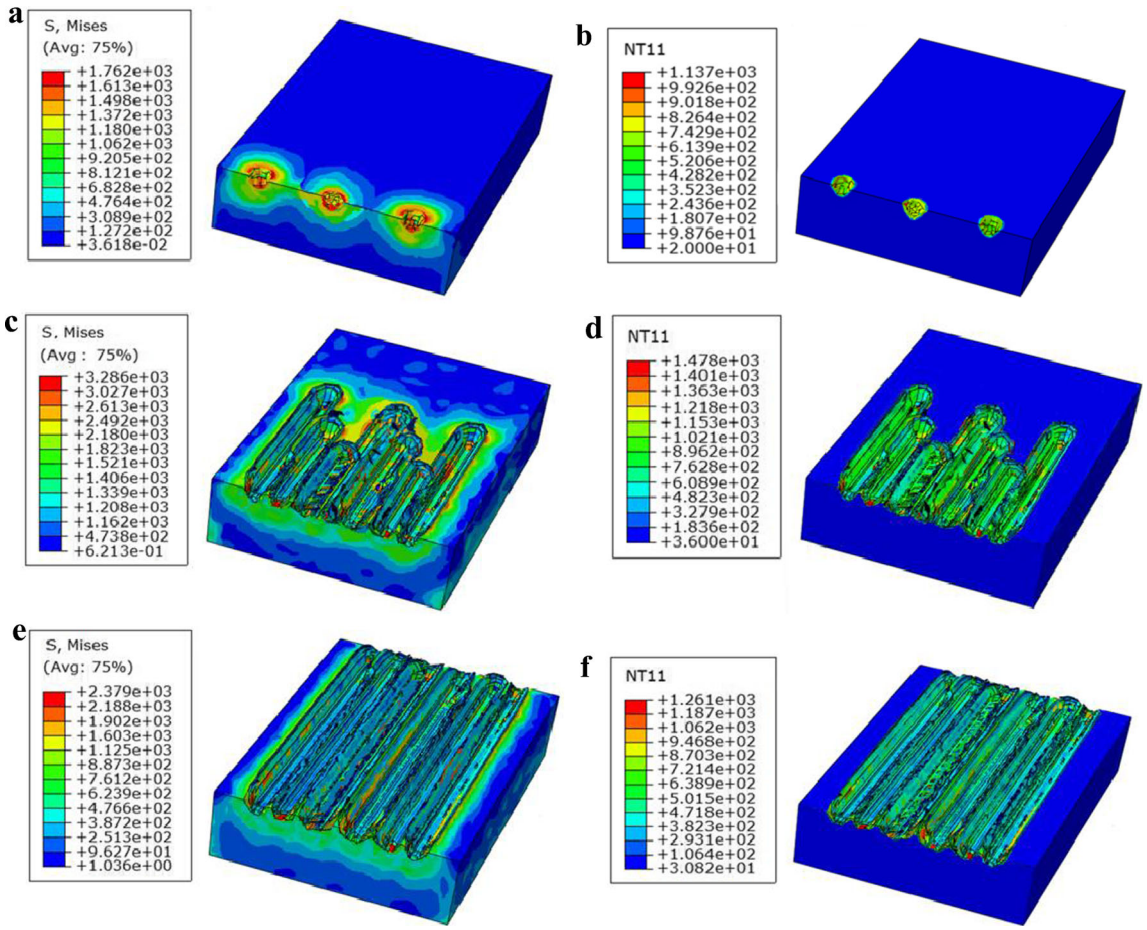

Fig. 8 Simulation of grinding process (Mises stress **a** cut-in, **c** the steady state, and **e** cut out; Temperature distribution fields **b** cut-in, **d** the steady state, and **f** cut out)

abrasive grains was simulated using ABAQUS. Figure 6a is CBN abrasive grains, whose shape is defined as a cone. The characteristic parameters of the grinding wheel abrasive are obtained by digital image processing technique and normal distribution, where height h is 120 μm, radius r is 61 μm, and cone angle θ is 72.61°. Figure 6b is a multi-particle model, and the size of the grinding wheel surface is 1000 × 1000 μm, which is distributed with multiple abrasive particles. Workpiece material of nickel base superalloy GH4169 was a cuboid with 2 mm in length, 1 mm in width, and 0.2 mm in height.

The simulation model established by ABAQUS is shown in Fig. 7. In this paper, abrasive arrangement angle β, lateral spacing Δx, and longitudinal spacing Δy are, respectively, compared and analyzed, under the certain condition of grinding speed and depth. Aurich et al. [20] indicate that the

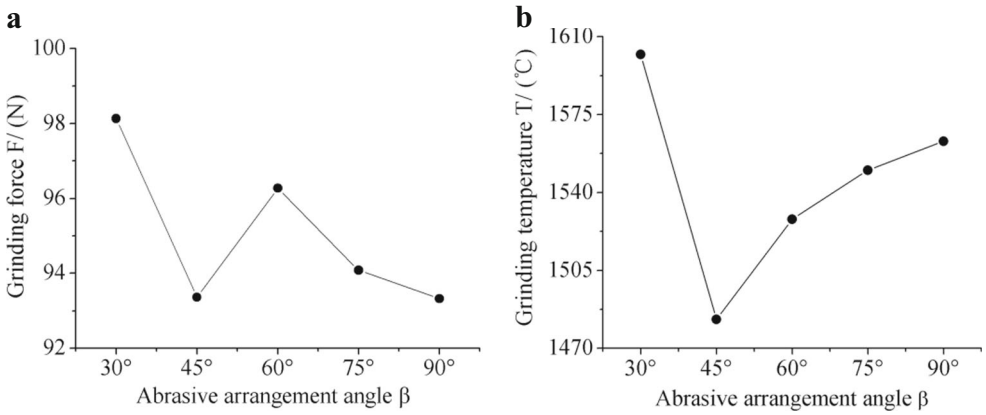

Fig. 9 The variation of force and temperature with the angle of beta. **a** F-β. **b** T-β

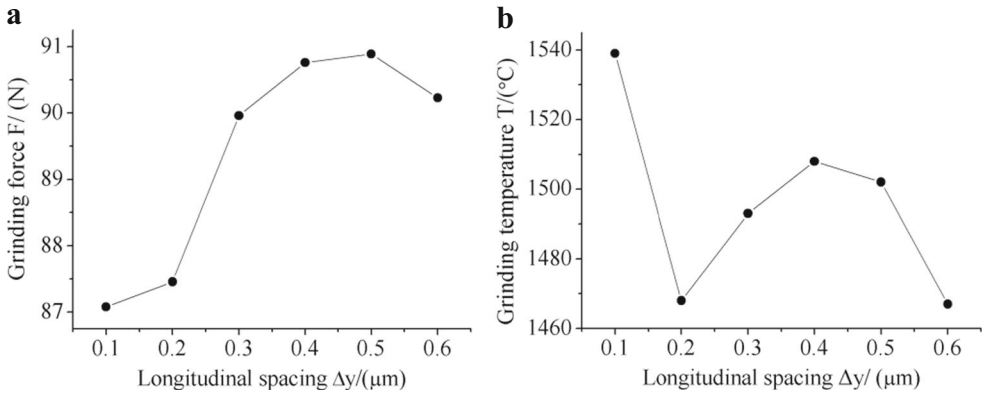

Fig. 10 The change of grinding force and temperature with abrasive grain spacing. **a** F-Δy. **b** T-Δy

transverse spacing Δx and the longitudinal spacing Δy should be less than 2 and 0.6 mm, respectively. In view of this, the distance between the abrasive grains was selected in the range of $\Delta x \leq 2$ mm and $\Delta y \leq 0.6$ mm under the conditions of given abrasive grain density. The abrasive grain arrangement angle β was selected in special angle. The simulation scheme is shown in Table 1.

The Mises stress and temperature distribution fields are shown in Fig. 8. As the abrasive grains cut into the workpiece from the initial stage to the steady state, material plastic deformation occurs, and the stress are gradually increased, which causes the heat to raise the temperature. It can be seen that stress and heat are concentrated in the processing area between abrasive and workpiece. When the abrasive grains are completely removed from the workpiece, the stress and temperature values are slowly reduced.

Under the condition of constant density of abrasive grains, the variation of force and temperature with the angle of beta is shown in Fig. 9. It can be seen that when the value of arrangement angle β is 45 or 90°, the grinding force is smaller than that of other angles. Meanwhile, the relatively low temperature occurs at 45°. The chip space between the abrasive particles is more uniform at $\beta = 45°$, which can promote the discharge of abrasive debris, thus weakening the friction effect, so that the grinding force decreases, and the heat generated by the material is reduced.

When the abrasive density is constant and $\beta = 45°$, the change of grinding force and temperature with abrasive grain spacing is shown in Fig. 10. It can be seen that when Δy increases (Δx decreases), the change of grinding force decreases after a rising firstly. The relatively small grinding force occurs at Δy of 0.1 and 0.2 mm, and grinding temperature is lower in Δy of 0.2 mm. By comprehensive comparison, when $\Delta y = 0.2$ mm ($\Delta x = 1.0$ mm), both the grinding force and the temperature are low.

It can be seen from the simulation that a relatively low grinding force and temperature can be obtained, when $\beta = 45°$, $\Delta x = 1.0$ mm, and $\Delta y = 0.2$ mm. Therefore, during the subsequent production of pressurized internal-cooling wheel, the parameters of regular grain distribution are arrangement angle of 45°, horizontal distance of 1.0 mm, and longitudinal distance of 0.2 mm.

3.1.3 Design of the internal-cooling channel

The channel diameter should be greater than the minimum stable flow diameter, in order to ensure the continuity of the coolant and

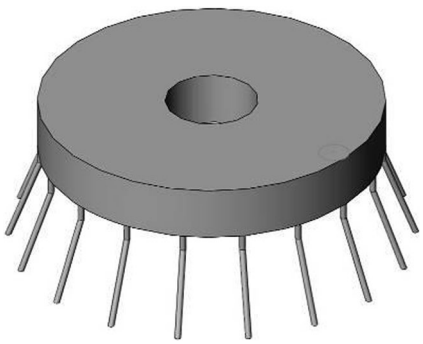

Fig. 11 3D simplified model of fluid domain

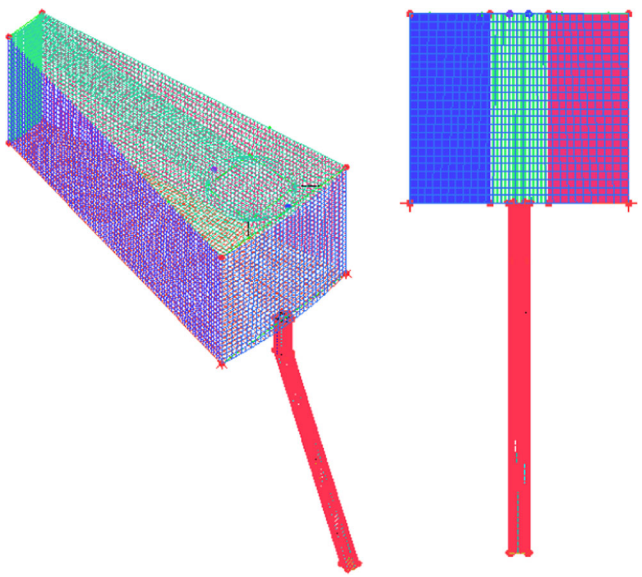

Fig. 12 Model mesh diagram

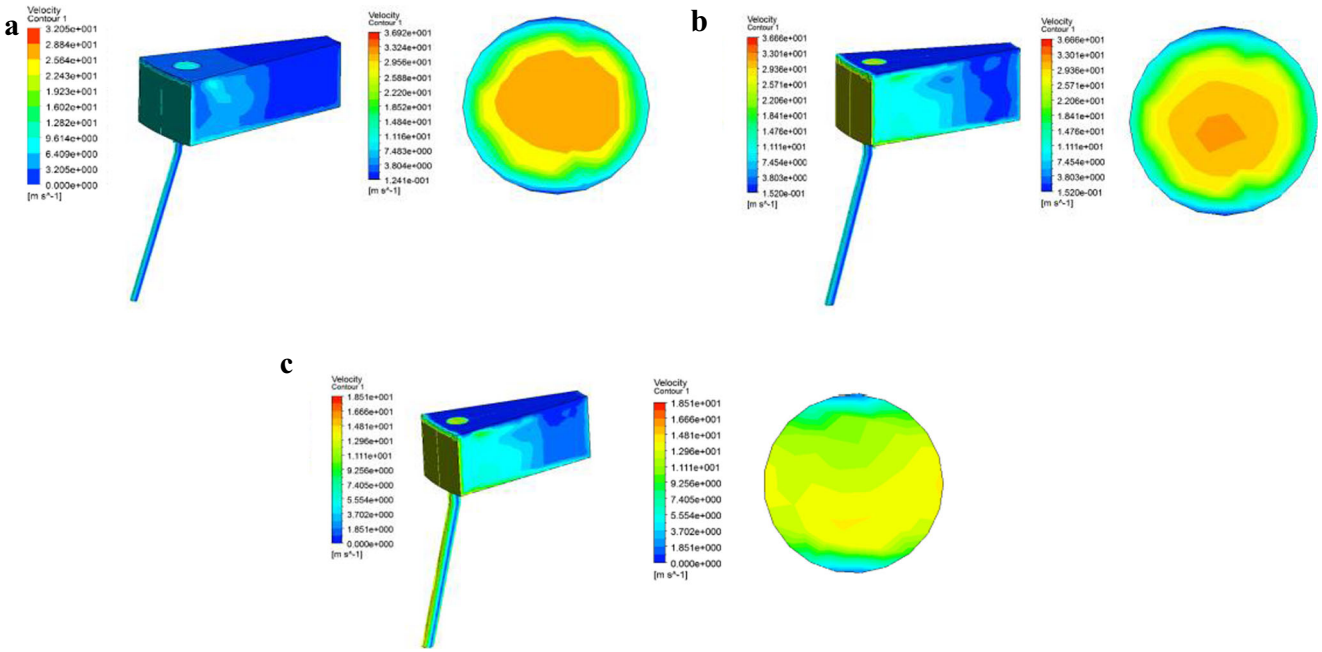

Fig. 13 Fluid velocity nephogram (left) and outlet velocity distribution (right) in different channel diameters of **a** $d = 1$ mm, **b** $d = 2$ mm, and **c** $d = 3$ mm. ($n = 2200$ r/min, $v_{in} = 3$ m/s)

achieve good cooling effect. Simultaneously, considering the processing technology of channel, the channel is too small to cause difficult processing, and too big to give rise to insufficient outlet flow, which results in poor cooling and low strength.

According to the formula proposed by Pijush [21], the s, h_w, and d criteria are expressed as follows:

$$s = \frac{8\left(\lambda/d + \sum\zeta\right)}{\left(\pi^2 d^2 g\right)} \tag{1}$$

$$h_w = sq^2 \tag{2}$$

$$d = \sqrt{4q/\pi v} \tag{3}$$

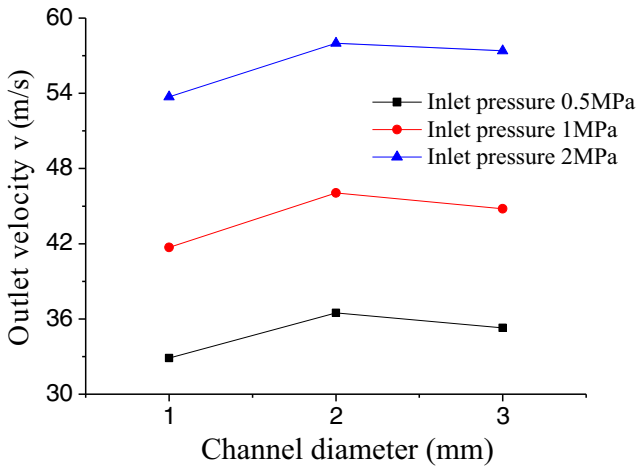

Fig. 14 The varying curve of maximum outlet velocity with the diameter of the channel ($n = 2200$ r/min)

Where d is the channel diameter (m), l the channel length (m), g the acceleration of gravity (m^2/s), s the channel impedance (s^2/m^5), q the coolant flow (m^3/s), v the coolant flow rate (m/s), h_w the head loss, λ the resistance coefficient, and $\sum\zeta$ the sum of the local resistance coefficient.

It can be guaranteed that the grinding fluid spray on the grinding area is continuous, when the channel diameter is larger than 0.8 mm. In addition, the oversize diameter of the channel is not conducive to the structural strength or the static and dynamic performance of the grinding wheel, considering that the channel is located inside the grinding wheel.

The fluid domain model is generated by Solidworks and imported into the ANSYS Workbench platform for meshing. The internal flow of fluid domain model is described by the energy conservation equation of fluid control. According to the actual working conditions of grinding operation, the model is simplified, and a few assumptions are presented in this article. Firstly, the flow inside the cavity is defined as turbulent flow. Secondly, the slight displacement deviation of the grinding wheel can be neglected due to the watershed is highly symmetrical. Thirdly, the channel outlet section is defined as the total outlet, where the leakage flow at the ring seal is not included. Ultimately, the influence of the heat transfer on the fluid is ignored, and the boundary condition of the wall is set to adiabatic boundary. A 3D model of the fluid domain is set up, as shown in Fig. 11. Since the fluid domain models is a rotation period symmetric model, the 1/18 model was taken for analysis. Considering the symmetry and periodicity of the model, at the same time, in order to improve the computational efficiency, the fluid domain model intercepts its 1/18 and meshes it, as exhibited in Fig. 12.

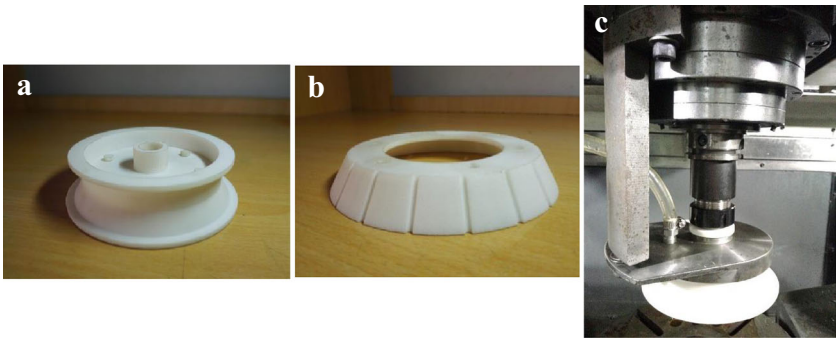

Fig. 15 3D printing model of the grinding wheel. **a** Upper matrix. **b** Lower matrix. **c** Assembly body.

The influence of channel diameter on flow velocity distribution was simulated by FLUENT, as shown in Fig. 13. In consideration of the size of the cutter in the process of manufacturing, this paper chose the channel diameter d of 1, 2, and 3 mm, and the rotating speed of 2200 r/min. The inlet boundary condition is defined as velocity-inlet of $v_{in} = 3$ m/s or pressure-inlet boundary condition. It can be seen in Fig. 13a that when $d = 1$ mm, the smaller coolant channel result in coolant to concentrate in the cavity. When $d = 2$ mm, the velocity distribution in the cavity is not sufficiently developed compared with the $d = 3$ mm. However, the buildup effect of fluid and the cavity pressure are both greater in d of 2 mm, and due to effect of internal pressure, the coolant is sprayed to the grinding area with faster flow rate in the channel, which can form a better heat transfer effect. From the fluid velocity nephogram in Fig. 13, it can been seen that the speed at outside of the cavity is greater than that at inside, and the speed changes obviously, because of the rotation of the grinding wheel. After the coolant flow into channel, the speed increases slowly. From the outlet velocity distribution cloud, we can see that the maximum outlet velocity is in the central area, and the center decreases toward the wall velocity, which is affected by the frictional resistance of the wall. As the diameter increases, the maximum velocity at the outlet reaches maximum when the channel diameter is $d = 2$ mm. The main reason is that the greater the diameter is, the lower the pressure is at the mold cavity, which reduces the rate of exports.

As can be seen in Fig. 14, with the increase of the channel diameter, the outlet velocity of the fluid increases first and then decreases, and the outlet velocity at the diameter of 2 mm is the largest. When the channel diameter is constant, the inlet pressure has a direct effect on the impact of the fluid, so that the outlet speed of the fluid increases. The main reason is that the greater the inlet pressure is, the greater the impact on the fluid is.

The parameters of the flow channel structure are preferably selected by the spraying velocity at the outlet of the channel. From the above, when the channel diameter is 2 mm, the larger internal pressure of the cavity and the smaller pressure loss in the flow process result in that the maximum outlet velocity is obtained. Greater coolant pressures in compression chamber can obtain a better heat transfer effect. Consequently, the final channel diameter is 2 mm.

3.2 3D printing model validation

The parts were printed by 3D printing molding in the light of the actual size of 1:1, according to the design of the grinding wheel structure, as shown in Fig. 15. Aiming at the technical characteristics of the static and dynamic sealing of the grinding wheel rotation, ring sealing was adopted, and sealing material was polytetrafluoroethylene (PTFE). Part models were assembled on the machine tool to verify the assembling effect of grinding wheels, fixture, and seal. The pressure system, injection effect of internal-cooling channel, and sealing situation were tested at the same time, as shown in Fig. 16. With the increase of rotating speed, the angle between linear directions

Fig. 16 Operation of the grinding wheel system with coolant supply. **a** $n = 200$ r/min. **b** $n = 500$ r/min. **c** $n = 800$ r/min

Fig. 17 Finite element mesh model

of coolant of channel outlet and horizontal plane becomes smaller. In grinding operation, outlet flow of cooling liquid was collected by using containers in a certain period of time. According to the continuity equation, fluid flow is the average fluid velocity multiplied by the pipe cross-sectional area. Therefore, it can be seen that outlet flow velocity of coolant can be controlled in a certain range by adjusting the inlet pressure of the coolant, and the jet impingement can be formed in order to achieve the purpose of forced heat transfer to the grinding zone.

The test results showed that the 3D grinding wheel model was well assembled, and both the pressure system and the grinding wheel operated faultlessly. The velocity of flow in flow nozzles could be proactively controlled via adjusting coolant flux, and the angle between linear directions of coolant of channel outlet and horizontal plane is small, which can achieve good cooling effect. No leakage of coolant occurs in grinding process, and the sealing effect was good, when the sealing ring was used.

3.3 Mechanical analysis of the grinding wheel matrix

The grinding wheel vibration will debase grinding accuracy and surface quality of workpiece and may even cause the grinding wheel rupture and damage of the machining system. The stability of the grinding system can be improved by avoiding resonance zone. The finite element model of the grinding wheel matrix was established to study the natural vibration characteristic of grinding wheels, as shown in Fig. 17. The ANSYS Workbench was used to make a modal analyze of grinding wheel. Figure 18 shows that the first-order natural frequency of grinding wheel matrix is 1131.8 Hz, which is higher than the maximum natural frequency of machine tool of 900 Hz. The results indicated that the grinding wheel was not easy to be destroyed on account of resonance in the grinding process.

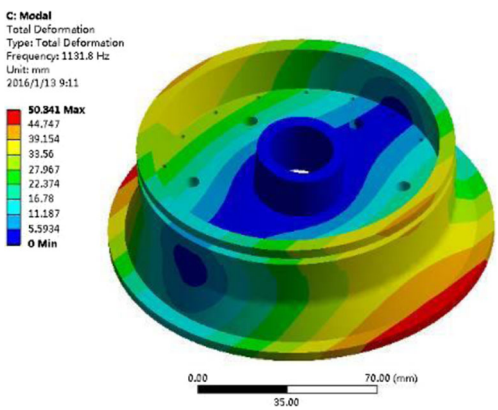

Fig. 18 The first-order mode shape diagram

Meanwhile, in order to calculate actual vibration amplitude and response of wheel matrix under the periodic load, and predict the continuous dynamic characteristics of structure, the harmonic response analysis was applied to research the matrix response under the action of axial and tangential excitation forces. Results illustrates that the low order natural vibration mode has a significant impact on the vibration of matrix. Obviously, modal analysis presents that resonant vibration does not occur at low natural frequencies, and the small displacement triggered by unidirectional vibration can make grinding wheels work safely and reliably.

As shown in Fig. 19, the stress analysis of the grinding wheel matrix was carried out, in order to avoid the stress concentration of the grinding wheel in the grinding process and ensure that the tensile strength exceeds the equivalent stress caused by the centrifugal force. It can be seen that the maximum centrifugal force on the outer ring of the grinding wheel is 36.2 MPa, which is much less than the strength limit of the grinding wheel matrix material. Therefore, the grinding wheel in the grinding process is safe in the test rotary speed.

3.4 Preparation of the grinding wheel matrix

Taking all the factors into account, this paper chose 45 steel materials to make various parts of the grinding wheel and its supporting fixture. The 45 steel materials not only reduces the weight of wheel body to a certain extent, which reduces the load of machine tool spindle rotation, but also increases the binding strength of the abrasive grinding wheel surface, due to the bonding effect between steel matrix and abrasive particles is better. Additionally, using 45 steel can effectively reduce and avoid thermal deformation of the grinding wheel caused by temperature rise in the grinding process, which further ensures that the grinding wheel has good grinding performance, for the reason that its coefficient of thermal expansion is low, as elaborated by Tang et al. [22]. The wheel end face was made of #80 CBN abrasive grains, and the area density of abrasives is 5.47/mm^2, according to the principle and structural design requirements of the pressurized internal-cooling slotted grinding wheel. The monolayer abrasive grains are uniformly brazed on the upper matrix of the grinding wheel. The matrix, the sealing ring, and the fixed connection of the

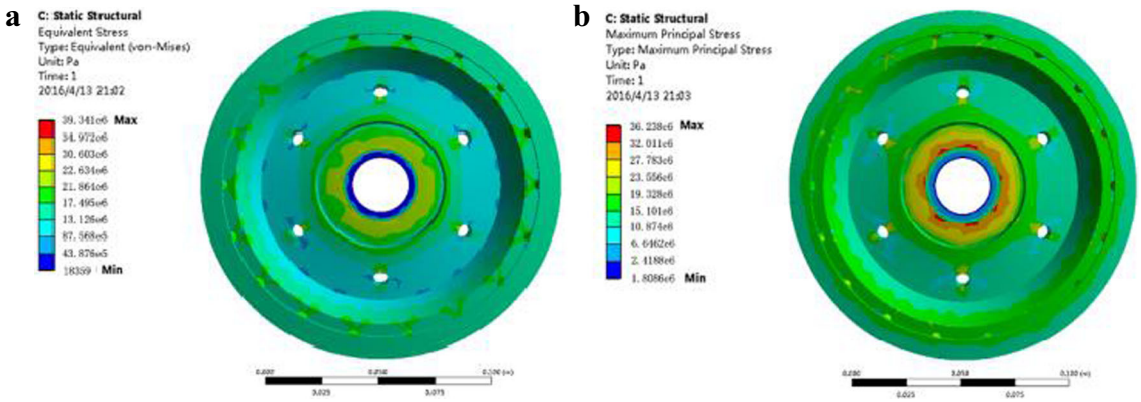

Fig. 19 Stress distribution nephogram of the grinding wheel. **a** Maximum principal stress nephogram. **b** Maximum shear stress nephogram

grinding wheel were prepared, as displayed in Fig. 20. The grinding wheel static balance experiment was carried out on machine tool. Simultaneously, this paper tested the sealing effect and pressurization effect after connecting the pressure system, as shown in Fig. 21, so as to ensure the safety and reliability of the wheels.

4 Experiments

4.1 Experiment conditions

Based on the single-factor design experiment scheme, the grinding performance of the grinding wheel was compared between the internal-cooling method and the external-cooling method, and the effectiveness of the internal-cooling method to improve the surface quality was verified.

Schematic of grinding experiment, which includes working platform, hydraulic system, dynamometric system, and temperature measurement system, is exhibited in Fig. 22. In the course of the experiment, firstly, the coolant is sent to the working platform through the hydraulic system, as displayed in Fig. 23. Afterwards, the flow rate of coolant can be controlled by adjusting the throttle valve control, and the coolant pressure value can be obtained through the pressure gauge, as shown in Fig. 24. When the coolant flows out from the bottom surface of the grinding wheel, the grinding wheel begins to grind the workpiece.

The experimental workpiece of nickel-based superalloy GH4169 was a pair of small blocks with 90 mm in length, 50 mm in width, and 10 mm in height. The testing machine was VMC30 five-axis CNC machine tools. The average temperature in the grinding process was measured by standard semiartificial type K thermocouple method. The JB-1C surface roughness tester was applied to measure surface roughness, and the surface micro-hardness was measured using a Vickers hardness meter. The surface micro-morphology was measured by KEYENCEVHX-500FE ultra-depth 3D microscope.

4.2 Experiment plan

In order to study the processing performance of nickel-based superalloy grinding under different cooling methods and different abrasive grain distribution conditions, the experiment was carried out by using single-factor test scheme. The grinding temperature and the surface quality including surface roughness, surface micro-hardness, and surface micro-structure were compared and analyzed under the condition of different grinding parameters. Grinding parameters is shown in Table 2. Each group of experiments was made with new workpiece. The data were measured three times in each group to obtain average value.

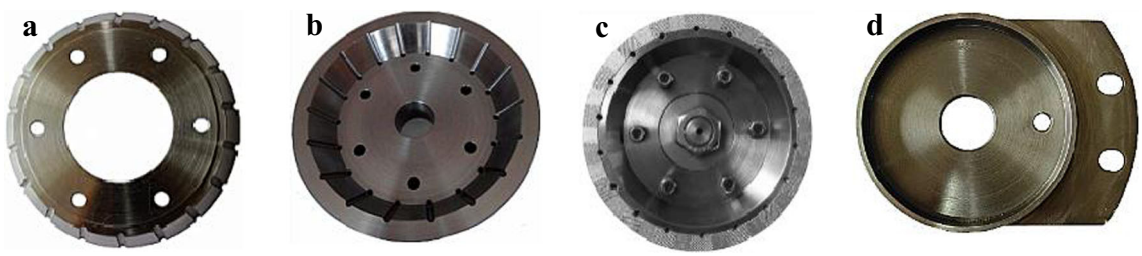

Fig. 20 Grinding wheel matrix. **a** Lower matrix. **b** Upper matrix. **c** Abrasive with ordered. **d** Cover plate

Fig. 21 Grinding wheel system with coolant supply

5 Results and discussion

5.1 Analysis of grinding temperature

The extent of heat accumulation in the arc area is reflected by the level of grinding temperature directly. In order to investigate the heat transfer effect on the pressurized internal-cooling grinding wheel, the grinding temperatures in different conditions, i.e., pressurized internal-cooling and external-cooling, were compared under the same grinding parameters, as shown in Fig. 25.

In general, compared to the external-cooling method, the pressurized internal-cooling method can leads to lower grinding temperature. With the increase of the grinding parameters, the heat transfer effect of the pressurized internal-cooling method was more significant. The coolant into the grinding arc efficiency was reduced with the increase of processing parameters, when the external-cooling method is used for grinding, resulting in a poor heat transfer effect, while using the pressurized internal-cooling method, coolant is directly sprayed to the abrasive grinding area, greatly improving the cooling fluid heat transfer efficiency and reducing the grinding temperature.

Figure 25a indicates that with the increase of rotating speed, the number of abrasive grains per unit time, friction, plastic deformation, and heat are increased, which gives rise to the increase of grinding temperature curve. Figure 25b illustrates that the grinding temperature in both cooling methods decreases with the increase of coolant pressure, but using internal-cooling method can achieve lower grinding temperature. It should be noted that the barrier effect is easy to produce with the increase of rotating speed, which has a significant influence on external injection coolant, resulting in only a small amount of coolant to enter the grinding zone. Nevertheless, pressurized internal-cooling method can improve the efficiency of heat exchange, because of the increase of centrifugal force. In summary, the heat transfer effect of pressurized internal-cooling method is more remarkable and effective.

5.2 Analysis of machined surface integrity

5.2.1 Analysis of surface roughness

Figure 26 reflects an influence of cooling method and coolant pressure on surface roughness with different processing parameters. The coolant was poured into the grinding arc better

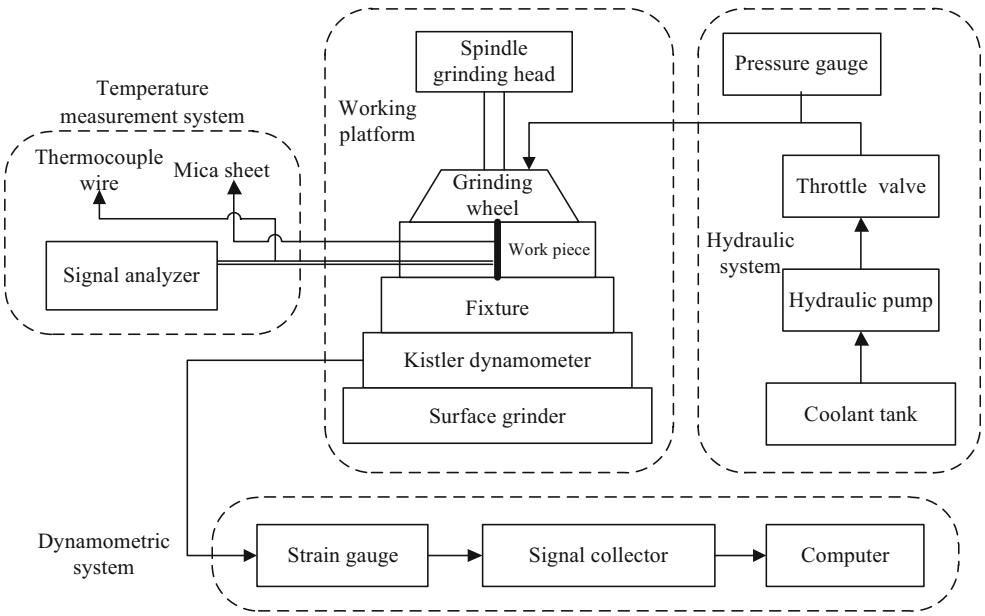

Fig. 22 Grinding wheel test platform

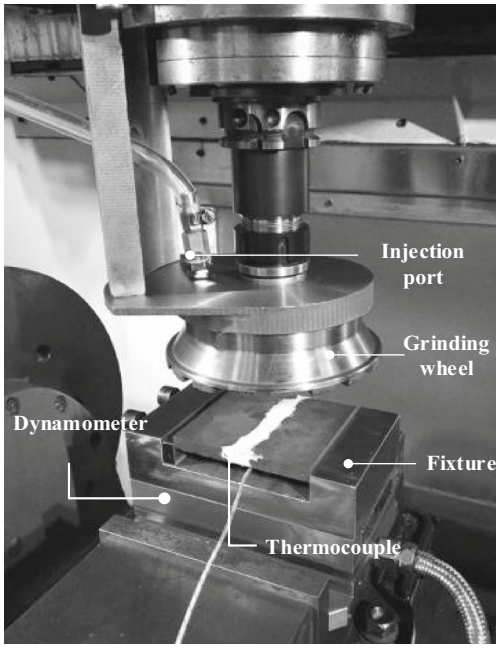

Fig. 23 Working platform

by using pressurized internal-cooling method, so that the heat transfer effect was obvious, and the scouring effect on both grinding debris and abrasive grains was more remarkable, which resulted in lower and smaller grinding temperature and surface roughness. As shown in Fig. 26a, the grinding thickness of single abrasive particle is reduced with the increase of grinding speed, resulting in the reduction of grinding surface roughness *Ra*. It can be seen in Fig. 26b that with the increase of coolant pressure, the surface roughness of workpiece is obviously reduced.

5.2.2 Analysis of surface micro-hardness

Figure 27 shows the hardness of the machined surface under different grinding parameters. In the grinding process, the

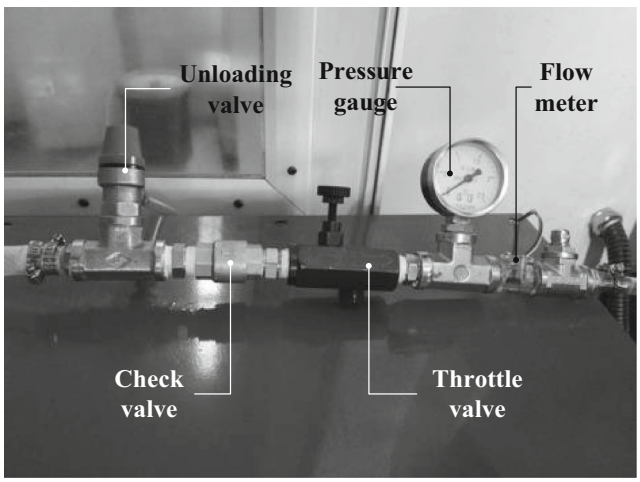

Fig. 24 Coolant supply control device

Table 2 Single-factor design experiment plan

Grinding parameter	Value	Cooling method
Rotating speed n/(r/min)	3000, 3500, 4000, 4500, 5000	Internal-cooling; external-cooling
Coolant pressure P/(MPa)	0.3, 0.43, 0.55, 0.68, 0.8	
Feed speed v_w/(m/s)	0.01	
Depth of cut a_p/(μm)	20	

essence of the workpiece surface hardening is the plastic deformation of the workpiece material, which is mainly reflected in the thermal strain caused by grinding heat and the mechanical strain caused by grinding force. As displayed in Fig. 27a, the micro-hardness of the machined surface increases evidently with the increase of the rotating speed, but the difference is not significant. Figure 27b illustrates that the micro-hardness can be decreased slightly with the increase of coolant pressure. Additionally, it can be seen from the figure that the lower surface hardness values can be obtained, due to the fact that the pressurized internal-cooling method can effectively reduce grinding heat and grinding force. Meanwhile, the increase of coolant pressure can reduce surface hardness of workpiece.

5.2.3 Analysis of surface morphology analysis

As elaborated by Ren et al. [23], nickel-based superalloy, as a typical difficult-to-machine material, is easy to adhere to the top of abrasive grain in the grinding process, so that the friction coefficient increases. At the same time, workpiece surface is easy to produce large deformation under the friction and extrusion of the abrasive grains, and the lattice of deformation zone is seriously distorted to produce higher grinding temperature. But the lower thermal conductivity of the material made the grinding heat to concentrate in the grinding surface easily, which brought about the formation of high grinding temperature and the local variation of surface organization; thus, it would develop grinding burn. Grinding burn is one of the most important factors that affect the quality of machined surface. The fatigue resistance of the workpiece can be greatly improved by effective control and suppression of grinding burn.

Figure 28 is the 3D shape of the grinding surface with different rotating speed under different cooling methods (magnification is ×500). Machining parameters were defined as follows: feed rate v_w was 0.01 m/s, grinding depth $a_p$was 20 μm, rotating speed n was 3000 r/min, and 4000 r/min.

Figure 28 indicates that the surface texture groove, obtained by the pressurized internal-cooling method, is clearer, neater, and more delicate than that of the external-cooling method under the same condition of rotating speed. The

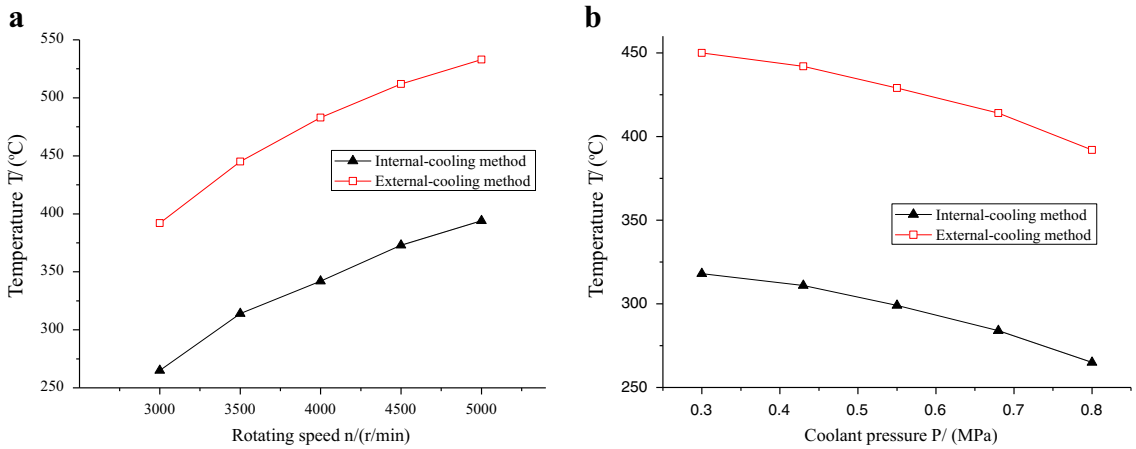

Fig. 25 Variation of grinding temperature under different cooling method with the change of grinding parameters. **a** The rotating speed. **b** Coolant pressure

change of rotating speed had a slight influence on the grinding texture of superalloy. When n = 3000 r/min, the surface of the grinding surface is clear and regular. As the rotating speed continues to increase to 4000 r/min, the smooth surface of workpiece can be obtained, and the scratches of abrasive are fine and relatively uniform. In the condition of the same grinding parameters, more stable grinding processing is achieved by using pressurized internal-cooling method, which can obtain more continuous and uniform surface morphology of material near the groove. The surface groove formed by external-cooling method has obvious breaking point or fluctuation, and the phenomenon of "grinding burn" occurs on the surface of workpiece.

Figure 29 shows the surface morphology of workpiece under different inlet pressure. Under certain coolant pressure, clear texture of machined surface and uniform surface color can be obtained by pressurized internal-cooling method. The grooves produced by abrasive sliding and plowing are obvious, and the greater the inlet pressure, the clearer the morphology. The results depict that the internal-cooling method can achieve good surface quality. It can be seen from the figure that the machined surface has a small bonding point, resulting in an instantaneous increase in the temperature of the arc area, which causes the workpiece material to bond and stay on the surface. Figure 29d is the machined surface topography of the workpiece obtained by dry grinding (i.e., coolant pressure is zero). Obviously, the surface of the workpiece has been burned, showing uneven brown and texture disorder, and metal bonding occurs at the groove edge.

Taking one with another, the heat transfer effect of pressurized internal-cooling method was better than that of external-cooling method, and the grinding temperature is lower than the latter under the condition of the same grinding depth, which improves grinding surface quality. With the increase of coolant pressure, the surface texture is more regular. Therefore, the pressurized internal-cooling grinding can obtain the good surface topography when using the appropriate processing parameters.

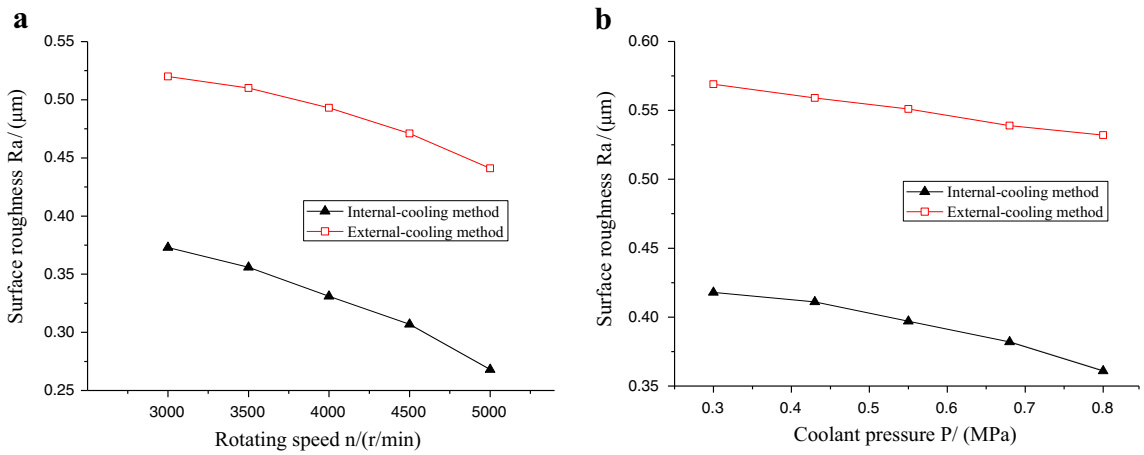

Fig. 26 Variation of surface roughness under different cooling method with the change of grinding parameters. **a** The rotating speed. **b** Coolant pressure

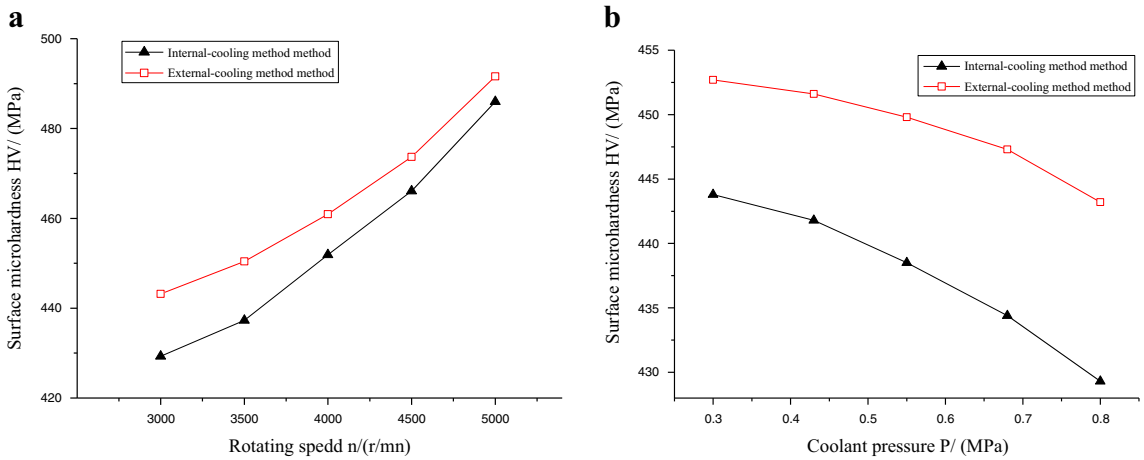

Fig. 27 Variation of surface micro-hardness under different cooling method with the change of grinding parameters. **a** The rotating speed. **b** Coolant pressure

6 Conclusions

In order to avoid the air barrier effect and then strengthen the heat transfer effect of coolant in grinding contact zone, a novel method of pressurized internal-cooling has been proposed, whose principle is that the supercharged coolant passes through small coolant channel inside the grinding wheel, and spray to the grinding arc zone with the higher outlet pressure from abrasive grain plane, and a pressurized internal-cooling slotted grinding wheel with abrasive orderly has been fabricated. The grinding wheel substrate, the internal-cooling system, and the comprehensive performance of the newly developed CBN wheel have been investigated. The creative conclusions can be drawn based on the simulation and experiment results:

1. Structure parameters are verified through the numerical simulation and 3D printing technology. The cooling cavity and flow channel are machined on the grinding wheel matrix, and the diameter of flow channel is 2 mm. The CBN abrasive grains were brazed at the grinding wheel end face with uniform interval arrangement, whose distribution parameters are arrangement angle of 45°, horizontal distance of 1.0 mm, and longitudinal distance of 0.2 mm.

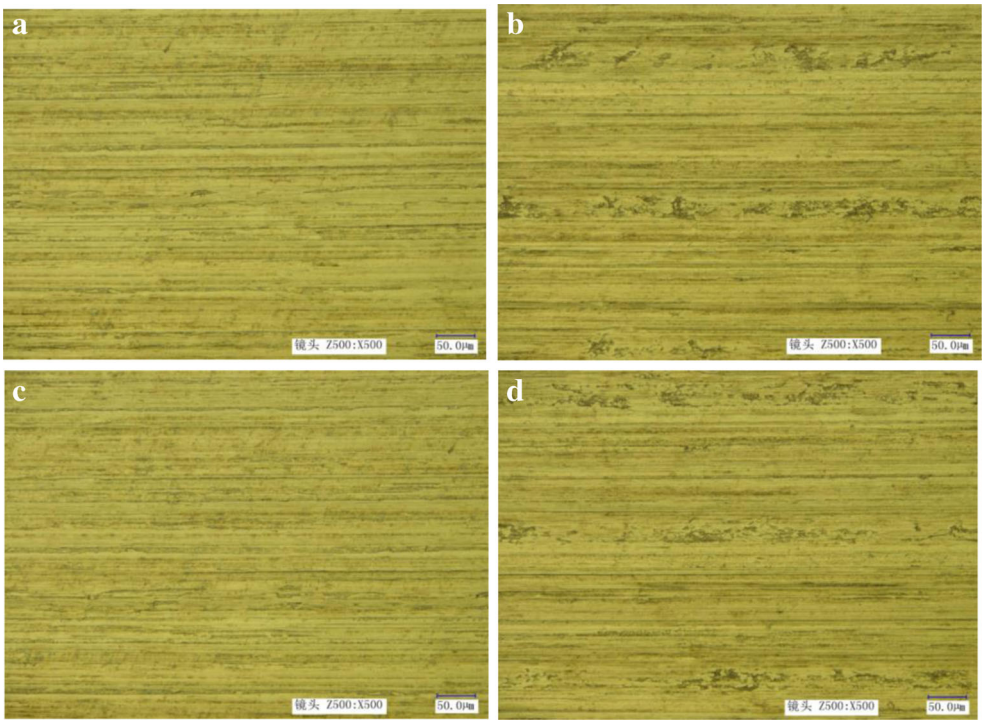

Fig. 28 Surface morphology of the workpiece after grinding (×500) under different cooling method with the same grinding parameters (v_w=0.01 m/s a_p=20 μm). **a**, **c** Pressurized internal-cooling method, n = 3000 and 4000 r/min. **b**, **d** External-cooling method, n = 3000 and 4000 r/min

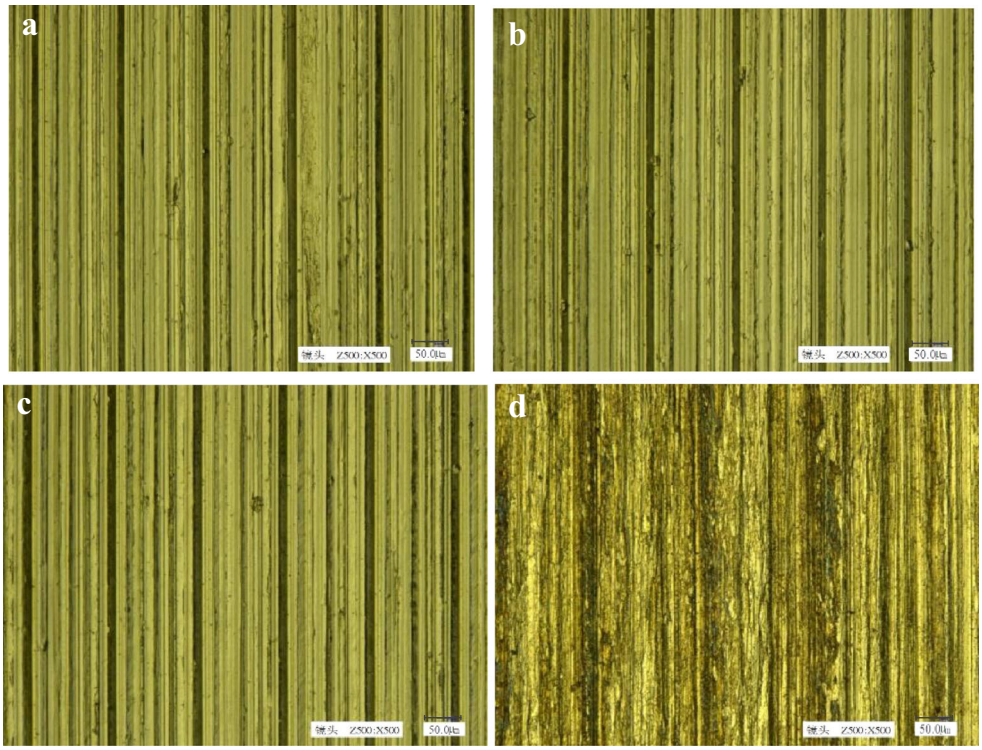

Fig. 29 Surface morphology of the workpiece after grinding (×500) under different inlet pressure (v_w=0.01 m/s, a_p=20 μm). **a** P = 0.8 MPa. **b** P = 0.5 MPa. **c** P = 0.2 MPa. **d** P = 0

2. Grinding performance of a brazed CBN grinding wheel for the grinding of GH4169 shows that under the same grinding parameters, the pressurized internal-cooling method has higher heat transfer efficiency, lower grinding temperature and surface roughness, more smooth and delicate surface, and better surface quality, by comparison with the traditional external-cooling method. Nevertheless, along with the increase of the grinding speed, the grinding temperature increases and the surface roughness decreases. The greater the coolant pressure is, the smaller the grinding temperature and surface roughness are, and the surface roughness Ra is 0.36~0.45 μm.

a_p, Grinding depth (μm); d, Channel diameter $d = \sqrt{4q/\pi v}$ (mm); F, Grinding force (N); g, Acceleration of gravity (m^2/s); h, Grain protrusion height (μm); h_w, Head loss $h_w = sq^2$; l, Channel length, m; n, Rotating speed (r/min); N, Slot number; P, Coolant pressure (MPa); q, Coolant flow (m^3/s); r, Grain radius (μm); Ra, Surface roughness; s, Channel impedance $s = \frac{8(\lambda/d+\sum\zeta)}{(\pi^2 d^2 g)}$, ($s^2/m^5$); T, Temperature; v, Coolant flow rate (m/s); v_{in}, Velocity-inlet (m/s); v_w, Feed rate (m/s); Δx, Lateral spacing (mm); Δy, Grain cone angle (mm); θ, Longitudinal spacing; η, Intermittent grinding ratio; β, Abrasive arrangement angle; λ, Resistance coefficient; $\sum\zeta$, Sum of the local resistance coefficient

Acknowledgements The authors would like to acknowledge the financial support from the National Natural Science Foundation of China (no. 51475404 and no. 11602212), the Natural Science Foundation of Hunan (no.13JJ8007), and the Hunan Provincial Cultivating Funds for Youth Backbone Teachers (no. 20151053008gg).

References

1. Ulutan D, Ozel T (2011) Machining induced surface integrity in titanium and nickel alloys: a review. Int J Mach Tools Manuf 51: 250–280
2. Ezugwu EO (2005) Key improvements in the machining of difficult-to-cut aerospace superalloys. Int J Mach Tools Manuf 45:1353–1367
3. Choudhury IA, El-Baradie MA (1998) Machinability of nickel-base super alloys: a general review. J Mater Process Technol 77: 278–284
4. Malkin S, Guo C (2007) Thermal analysis of grinding. CIRP Ann Manuf Technol 56:760–782
5. Brinksmeier E, Heinzel C, Wittmann M (1999) Friction, cooling and lubrication in grinding. CIRP Ann Manuf Technol 48:581–598
6. Chen ZT, Chen WY (2011) Suppression of surface burn in grinding of titanium alloy TC4 using a self-inhaling internal-cooling wheel. Chin J Aeronaut 24:96–101
7. He QS, Fu YC, Xu HJ, Ma K, Chen C (2013) Development of annular heat pipe grinding wheel for high efficiency machining of TC4 titanium alloy. Acta Aeronaut Astronaut Sin 4:1740–1747
8. Shi C, Xun L, Chen Z (2014) Design and experimental study of a micro-groove grinding wheel with spray cooling effect. Chin J Aeronaut 27:407–412
9. Nadolny K (2015) Small-dimensional sandwich grinding wheels with a centrifugal coolant provision system for

traverse internal cylindrical grinding of steel 100Cr6. J Clean Prod 93:354–363
10. Aurich JC, Kirsch B, Herzenstiel P, Kugel P (2011) Hydraulic design of a grinding wheel with an internal cooling lubricant supply. Prod Eng 5:119–126
11. Ding WF, Xu JH, Chen ZZ, Su HH, Fu YC (2010) Wear behavior and mechanism of single-layer brazed CBN abrasive wheels during creep-feed grinding cast nickel-based superalloy. Int J Adv Manuf Technol 51:541–550
12. Chen ZZ, Xu JH, Ding WF, Ma CY, Fu YC (2015) Grinding temperature during high-efficiency grinding Inconel 718 using porous CBN wheel with multilayer defined grain distribution. Int J Adv Manuf Technol 77:165–172
13. Ding WF, Xu JH, Chen ZZ, Yang CY, Song CJ, Fu YC (2013) Fabrication and performance of porous metal-bonded CBN grinding wheels using alumina bubble particles as pore-forming agents. Int J Adv Manuf Technol 67:1309–1315
14. Yu H, Wang J, Lu Y (2016) Simulation of grinding surface roughness using the grinding wheel with an abrasive phyllotactic pattern. Int J Adv Manuf Technol 84:861–871
15. Ding WF, Barbara L, Zhu YJ, Li Z, Fu YC, Su HH, Xu JH (2017) Review on monolayer CBN superabrasive wheels for grinding metallic materials. Chin J Aeronaut 30:109–134
16. Oliveira JFG, Bottene AC, Franca TV (2010) A novel dressing technique for texturing of ground surfaces. CIRP Ann Manuf Technol 59:361–364
17. Courbon C, Kramar D, Krajnik P, Pusavec F, Rech J, Kopac J (2009) Investigation of machining performance in high-pressure jet assisted turning of Inconel 718: an experimental study. Int J Mach Tools Manuf 49:1114–1125
18. Peng RT, Tang H, Tang XZ, Tan YQ, Zhou Z An internal-cooling grinding wheel, China Patent ZL201410197728.8, August 6, 2014.
19. Ghosh A, Chattopadhyay AK (2007) On cumulative depth of touch-dressing of single layer brazed CBN wheels with regular grit distribution pattern. Mach Sci Technol 11:259–270
20. Aurich JC, Braun O, Warnecke G, Cronjäger L (2003) Development of a super abrasive grinding wheel with defined grain structure using kinematic simulation. CIRP Ann Manuf Technol 52:275–280
21. Kundu PK, Cohen IM, Dowling DR (2012) Fluid mechanics, Fifth edn. Elsevier, Amsterdam
22. Tang YL, Liang YC, Huo DH, Chen K (2003) Study on nanometric cutting mechanism of monocrystalline silicon by molecular dynamics. Microfabrication Technol 2:76–80. Chinese
23. Ren JX, Kang RK, Wang XB (2011) Grinding technology of difficult-to-machine. Publishing House of Electronics Industry, Beijing